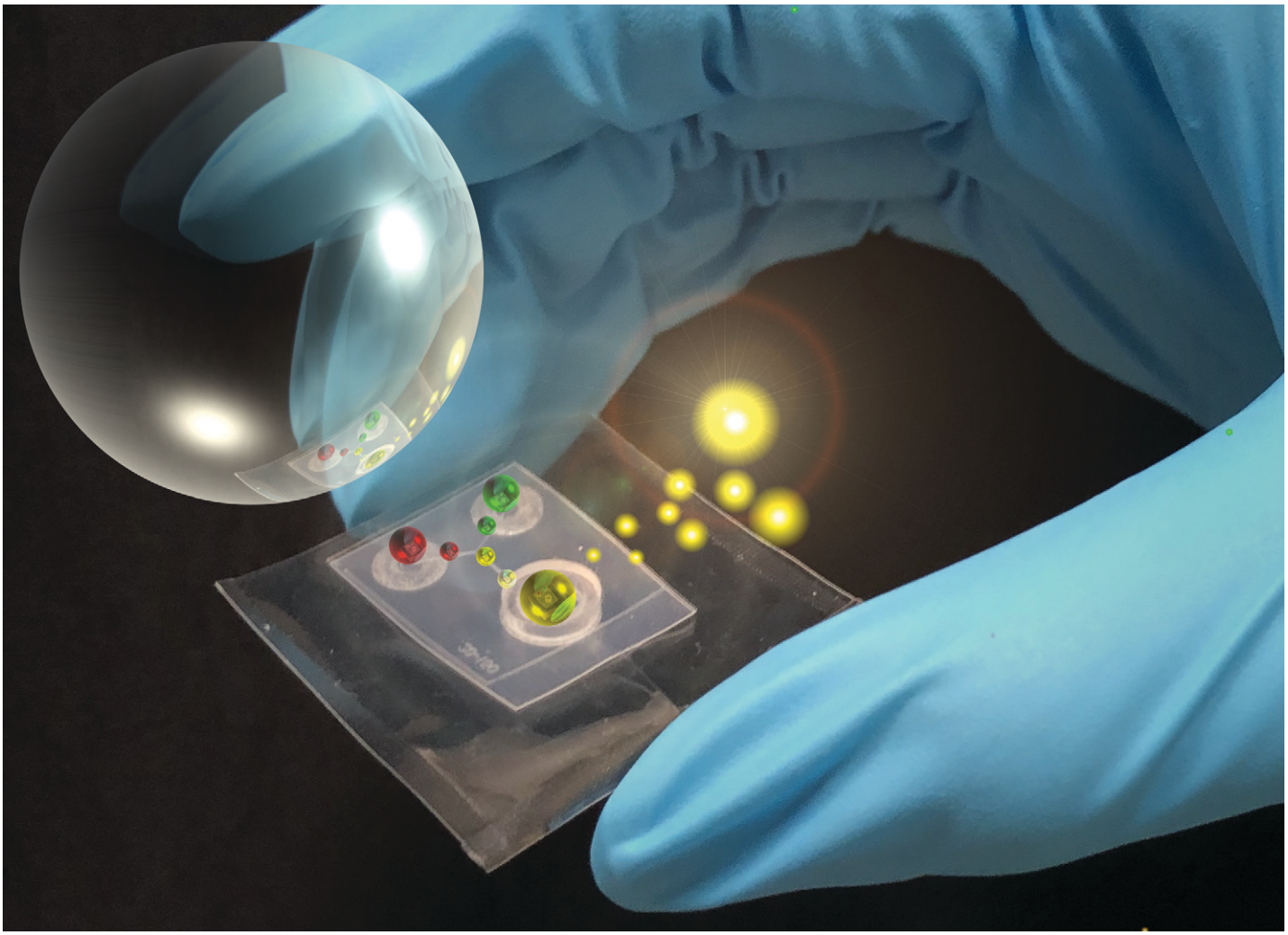

Featuring work from the Biomechanical Microsystems Laboratory of Professor Yu-Hsiang Hsu, Institute of Applied Mechanics, National Taiwan University, Taipei, Taiwan (R.O.C).

Vacuum pouch microfluidic system and its application for thin-film micromixers

A vacuum pouch microfluidic system is developed for on-site detections. This system uses laminated plastic films to incorporate a microfluidic device and a vacuum pouch which serves as an on-chip pump. It is a user-friendly device for on-site detection with advantages of being standalone and portable, lightweight and flexible, disposable and low cost, with a long shelf-life.

As featured in:

See Cheng-Je Lee and Yu-Hsiang Hsu, *Lab Chip*, 2019, **19**, 2834.

ROYAL SOCIETY OF CHEMISTRY | Celebrating IYPT 2019

rsc.li/loc

Registered charity number: 207890

Lab on a Chip

PAPER

Cite this: *Lab Chip*, 2019, **19**, 2834

Vacuum pouch microfluidic system and its application for thin-film micromixers†

Cheng-Je Lee and Yu-Hsiang Hsu *

Received 25th November 2018,
Accepted 16th July 2019

DOI: 10.1039/c8lc01286e

rsc.li/loc

In this paper, a new type of lab-on-a-chip system, called vacuum pouch microfluidic (VPM) system, is reported. The core of this technology is a thin-film vacuum pouch that provides negative pumping pressure once it is activated. It is a degassed plastic bag that encloses a microfluidic chip. To demonstrate its performance, a passive thin-film micromixer is developed to integrate with the vacuum pouch. Since both the vacuum pouch and the thin-film micromixer are made of plastic film, they can be laminated together to construct a multi-layered microfluidic system. Excluding the storage reservoir, the overall thickness is 0.4 mm and the total weight is 0.3 g. This system provides a simple and straightforward strategy to construct a standalone, portable, flexible and low cost microfluidic system. The thin-film micromixer uses a serpentine channel to perform the mixing process, and it is found to have distinct mixing mechanisms under different Reynolds (Re) numbers, where lateral diffusion dominates for $Re < 1$ and chaotic mixing starts to contribute for $Re > 10$. Integrating this thin-film micromixer with the vacuum pouch, it is demonstrated that the negative pumping pressure can be adjusted by different storage reservoirs being placed at the channel exit. Reynolds numbers ranging from 0.0064 to 45.2 can be achieved. It also is verified that the VPM micromixer can be stored for 4 weeks to provide a sufficient flow rate for mixing applications. Finally, to demonstrate the feasibility of applying this VPM-based thin-film micromixer for on-site detection, this system is integrated with the colorimetric method. It is verified that a 10 μl ferrous ion solution and a 10 μl potassium ferricyanide solution can be mixed in 12 seconds, and concentrations of 10 ppm to 1000 ppm can be quantified by analyzing the colorimetric signal in hue values.

1. Introduction

Lab-on-a-chip devices have been recognized as potential tools for on-site collection and in-field detection for point-of-care diagnostics,[1–3] environmental analysis[4,5] and food safety.[6,7] They provide a means to perform qualitative and quantitative analysis with a minimal requirement for end users to understand the driving mechanism and operation procedures. To meet this requirement, many self-contained microfluidic systems have been developed. A comprehensive review can be found in ref. 8. This type of system can be separated into three major groups: active, hand-powered and passive. The active group of chip-based detection systems usually incorporates a portable system for automatic processing, detection and analysis. These portable systems are usually designed to perform intricate fluidic handling and operations through well-engineered pumping and valving devices. They rely on the precision assembly of multiple actuators with loaded chips, such as pressurized tubes, electrical control cables, electrical power sources and mechanical actuators. These approaches provide precision operations and simple user interfaces. Nevertheless, the overall system cannot be very small and a battery or a power source is needed for operation.[1]

More portable or embedded pumping methods have also been reported for hand-powered self-contained microfluidic systems. For example, a finger-powered microfluidic pump can be embedded on a chip by incorporating a deformable chamber.[9] The pumping area is large enough for activation by a fingertip. A similar concept has also been reported for microfluidic valves using a deformable chamber with a pillar that can be pressed down manually to activate a check valve for opening a vacuum chamber.[10] Hand-powered mechanical features that can be integrated directly with microfluidic devices have also been reported. For example, a miniature syringe can be integrated with a microfluidic chip.[11] Also, a latex balloon pressure pump can be installed to load reagents.[12] Another method is to use the lid of the reagent reservoir to create a volume change in the top air cavity for generating positive or negative pumping pressure for liquid manipulation.[13]

Institute of Applied Mechanics, National Taiwan University, No. 1, Sec. 4, Roosevelt Rd., Taipei 10617, Taiwan, ROC. E-mail: yhhsu@iam.ntu.edu.tw

† Electronic supplementary information (ESI) available. See DOI: 10.1039/c8lc01286e

On the other hand, the passive self-contained microfluidic system is usually designed for single use processes. For example, the high porosity of polydimethylsiloxane (PDMS) has been applied for embedding a vacuum pump on a chip by evacuating air from the PDMS device before use.[14] Capillary force has also been applied to pump reagents for paper-based devices using patterned hydrophilic paper.[15–18] A recent review of paper-based technologies can be found in ref. 19.

Ideally, a microfluidic device for on-site detection should have a user-friendly interface and should be lightweight for portability. To meet these requirements, we developed a vacuum pouch microfluidic (VPM) system that is stand-alone, self-powered, lightweight, disposable, and low cost and that has an easy-to-use interface. The fabrication process of this VPM system is based on two industrial processes for plastic thin films: hot embossing and vacuum pouch packing. The microfluidic channels and chambers were hot embossed into a polypropylene (PP) plastic film and sealed with another vacuum seal bag to construct a thin-film microfluidic device. This VPM device could be activated easily once the vacuum pouch was pierced open with needles at designated locations connected to loading channels of the enclosed thin-film microfluidic device. To make this VPM system a user-friendly device, the passive microfluidic design was used. Thus, the VPM system can operate by itself once it is activated by releasing negative pressure stored in the vacuum pouch, making it a user-friendly device.

In this paper, we report our study on developing a VPM device for mixing applications. Since laminar flow dominates microfluidic systems and pressure applied at the entrance or exit is the driving source, diffusion and geometrically induced chaotic advection are the two major mixing mechanisms. Reported data suggest that the transition from diffusive to chaotic mixing is roughly at Re = 1 and Pe = 1000.[20] Among reported passive micromixers,[21] the serpentine channel is one of the most common microfluidic mixers.[22,23] It has a clear separation of mixing mechanisms over 3 orders of Reynolds number.[23] We adopted this concept to develop a thin-film micromixer for easy integration into the vacuum pouch. Some of the finite element analysis and experimental studies on the serpentine micromixer were presented in two conference papers.[24,25] Preliminary studies on the VPM micromixer was also discussed in ref. 25. Here, we provide a complete study on the VPM-micromixer with detailed experimental studies and data analysis. To demonstrate the performance of the VPM-based thin-film micromixer (VPM micromixer), the flow rate during loading was investigated. The back pressure induced by the storage reservoir was designed to generate 4 orders of flow rates and Reynolds numbers. Both diffusive and chaotic mixing mechanisms can be achieved. Then, the capability for long-term storage was studied for 28 days. Finally, the developed VPM micromixer was applied to detect the concentration of heavy metal ions in an aqueous solution *via* a colorimetric detection method. The feasibility of using this VPM micromixer for on-site detection was verified.

2. Materials and methods

Design of the VPM micromixer

The design concept of the VPM micromixer is illustrated in Fig. 1A and B, and Fig. 1C–E show three different designs to control the flow rate. The basic configuration was a 22 mm long by 18 mm wide by 0.25 mm thick PP thin-film micromixer sealed inside a 35 mm long by 35 mm wide by two-layered 0.075 mm thick PP vacuum pouch. Commercial vacuum seal bags made by Food Saver® were also used. At the two reagent loading areas, the inner surface of the vacuum pouch was adhered to the surface of the thin-film micromixer to create a seal (Fig. 1C–E: grey seal), and the exit of the micromixer was open to the inner cavity of the vacuum pouch, which was under vacuum. A storage reservoir with a 5 mm inner diameter and an 8 mm outer diameter was placed at the exit of the micromixer between the vacuum pouch and the thin-film micromixer for adjusting the level of negative pressure during activation. This storage reservoir can also be used to store mixed solution for post-processing.

Thus, using this passive micromixer, the operation process only had two steps. First, the two reagents to be mixed were loaded at the two entrances of the micromixer on the surface of the vacuum pouch (Fig. 1A). Then, needles were used to pierce through the vacuum pouch underneath reagents for activating the mixing process. Since the vacuum pouch and the microchannel of the micromixer were under vacuum, reagents were sucked into the micromixer once the vacuum pouch was pierced open (Fig. 1B). The driving pressure came from the pressure difference between the external atmospheric pressure and evacuated negative pressure inside the microchannel and vacuum pouch. To control the induced flow rate during loading, the pumping pressure can be adjusted by the design of the storage reservoir.

The relationship between the driving pressure (ΔP) and the volume flow rate (Q) can be expressed as:[26]

$$\Delta P = R_{\mathrm{H}} Q, \tag{1}$$

where R_{H} represents the total hydraulic resistance of the microchannel and the vacuum pouch. For a rectangular microchannel with a width larger than the height, the hydraulic resistance under laminar flow can be approximated as:[26]

$$R_{\mathrm{H}} = \frac{12\eta L}{\left[1 - 0.63\left(h/w\right)\right]} \frac{1}{wh^3}, \tag{2}$$

where L, h, w and η represent the length, height and width of the microchannel and the viscosity of the liquid, respectively. It shows that the hydraulic resistance can be adjusted by the cross-sectional geometry and the length of the microchannel. On the other hand, the residual air remaining inside the cavity (V_{T}) of the microchannel and the storage reservoir provided additional back pressure during loading. Once reagents started flowing into the microchannel, residual air was

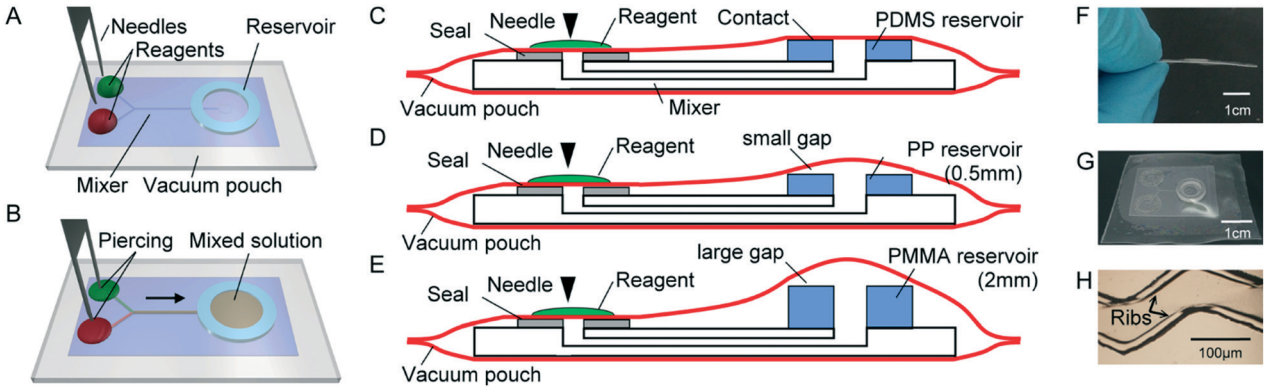

Fig. 1 (A and B) Illustrations of the design and operation of the VPM micromixer, where step 1 is to load reagents (A) and step 2 is to activate the VPM micromixer by needles (B). (C–H) Illustrations of the VPM micromixer in three different driving modes, including low LP- (C), medium MP- (D) and high HP- (E) pumping modes. (F and G) Pictures of fabricated devices. (H) A micrograph of the vacuum seal bag made by Food Saver®.

pushed and compressed into the reservoir. The decrement of volume $V(t)$ inside the microchannel and reservoir can be expressed as:

$$V(t) = V_{\mathrm{T}} - \int_0^t Q(\tau)\,\mathrm{d}\tau, \tag{3}$$

where $Q(\tau)$ represents the volume flow rate at time τ after loading. Using the ideal gas law, eqn (1) can be written as the following equation to describe the loading process:

$$\Delta P(t) = P_{\mathrm{atm}} - \frac{nRT}{V(t)} = R_{\mathrm{H}} Q. \tag{4}$$

where P_{atm} is the atmospheric pressure. Thus, a larger reservoir results in a smaller change of $V(t)$ and a smaller reduction rate of driving pressure $\Delta P(t)$.

Applying this concept, three different driving modes of the VPM micromixer were designed based on eqn (4) and are shown in Fig. 1C–E. Fig. 1C shows the design of the low pressure mode (LP). The reservoir (blue box) was made of a 0.5 mm thick PDMS ring that was adhered to the surface of the thin-film micromixer at the exit. It made conformal contact with the inner surface of the vacuum pouch, creating a large back pressure and resulting in a low driving pressure. Fig. 1D shows the design of the medium pressure mode (MP). The reservoir (blue box) was made of a 0.5 mm thick PP reservoir. It created a small gap between the vacuum pouch and the PP reservoir, and a lower back pressure was created to generate a medium driving pressure. A much higher pressure gradient, the high-pressure mode (HP), can be created using a 2 mm thick PMMA reservoir (blue box) that left a large gap and resulted in a high flow rate, as shown in Fig. 1E. Fig. 1F and G show two pictures of the VPM micromixer. The two circular rings around the two entrances were adhesives separating the evacuated vacuum pouch from the loading area. The overall thickness is 0.4 mm except the reservoir area, and the overall weight was only 0.3 g. Finally, a magnified picture of vacuum seal bags made by Food Saver® is shown in Fig. 1H. It has ribs designed on the inner surface of the plastic bags to enhance gas evacuation efficiency during the sealing process. We used these vacuum seal bags for the study of long-term storage and the influence of viscosity on the pump performance.

Design of the serpentine micromixer

The configuration of the passive micromixer is shown in Fig. 2A. A standard Y-shape micromixer was used. The two reagent loading channels were 5 mm in length by 100 μm in width by 60 μm in height. This design provided a sufficient length to develop laminar flow and was long enough to prevent cross-contamination between loaded reagents on the surface of the vacuum pouch. The serpentine mixing channel was 8 mm in length by 200 μm in width by 60 μm in height. Ten or twenty obstacles were embedded in the mixing channel to construct the serpentine microchannel, as shown in the magnified image in Fig. 2A. The total length for 10 and 20 obstacles was 1.4 mm and 2.9 mm, respectively. The widths of the serpentine channel and turning point were 100 μm and 50 μm, respectively. The number of obstacles also determined the hydraulic resistance of the serpentine channel, as described in eqn (2). The mixing mechanism can be diffusive or chaotic advection, depending on the flow rate and the resulting Reynolds number (Re).[23] At high Re values, the fluidic flow can be chaotic starting from right corners. This effect can enhance the mixing efficiency. On the other hand, the mixing performance can be high at low Re values since the flow rate is slow and there is sufficient time for lateral diffusion. Between these two extreme conditions, the mixing efficiency is much lower.

This dependency on the flow rate was investigated by finite element analysis (FEA) and experimental studies. The volume flow rate Q used in this study ranged from 1 μl min^{-1} to 500 μl min^{-1}, resulting in Reynolds numbers ranging from 0.13 to 66.67. FEA results were compared with trajectories of red-fluorescent 1 μm polystyrene beads (Sigma-Aldrich L2778) flowed inside a PDMS molded serpentine micromixer driven by two syringe pumps (New Era, NE-1000) *via* two 15 cm long stainless steel needles. The correlations between the flow pattern and mixing performance were studied, and the

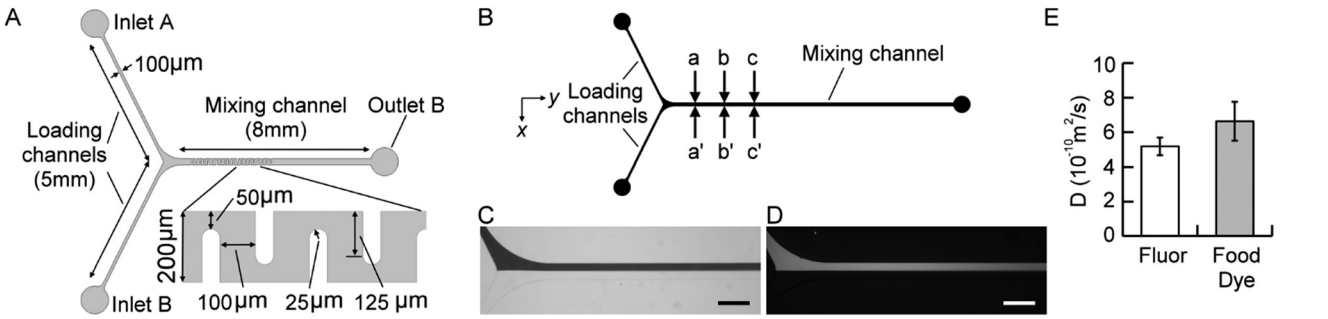

Fig. 2 (A and B) Illustrations of the serpentine micromixer (A) and the Y-shaped mixer for measuring diffusivity (B). (C–E) Experimental results of food dye (C), fluorescein solution (fluor) (D) and measured diffusivity D (E) (scale bar = 400 μm).

dependency on the Re value was also investigated. Discussion on the finite element analysis and experimental verification is provided in the ESI.† FEA results suggest that the mixing mechanism of this serpentine micromixer was diffusion dominated for Re $<$ 1 and chaotic advection dominated for Re $>$ 10 (Fig. S1†). This biphasic mixing performance was also verified further using a PDMS micromixer with an identical serpentine channel, and experimental results confirmed the FEA findings (Fig. S2 and S3†). The identified performance of this serpentine micromixer was applied to the design and verification of the VPM micromixer.

Diffusivity measurement

The diffusivities of food dye and fluorescein solution (Sigma-Aldrich F6377) used in this study were first measured using a Y-shaped mixing microchannel, as shown in Fig. 2B. The width and height of the Y-shaped microchannel were 200 μm and 50 μm, respectively. Diluted food dye or 5 μg ml^{-1} fluorescein solution in DI-water was pumped into one of the loading channels by a syringe pump, and the other one was flowed with DI-water at an identical flow rate by another syringe pump. The flow rate was set at 5 μl min^{-1} for both pumps to maintain laminar flow in the microchannel and to make diffusion the dominant mass transport. Thus, molecules diffused perpendicularly to the flow direction and could be used to measure diffusivity.

According to Fick's second law, the concentration gradient $c(x,t)$ across an interface between two liquids is

$$c(x,t) = \frac{c_0}{2} + \frac{c_0}{2}\mathrm{erf}\left(\frac{x}{\sqrt{4Dt}}\right), \quad (5)$$

where x and t are the lateral direction and the elapsed time, respectively. D and c_0 represent the diffusivity and the original concentration, respectively. The error function erf(x/x') is expressed as the following formula:

$$\mathrm{erf}\left(\frac{x}{x'}\right) = \frac{2}{\sqrt{\pi}}\int_0^{x/x'} e^{-t^2}\mathrm{d}t. \quad (6)$$

Using eqn (5), the measured concentration profile across the microchannel can be curve-fitted to measure diffusivity. To accurately measure diffusivity, three different locations of the diffusive mixing channel at 2 mm (a–a′), 4 mm (b–b′) and 6 mm (c–c′) were measured and curve-fitted (Fig. 2B). These three different locations represented 3 sequential time points (t) of the diffusion process. Fig. 2C and D show the corresponding experimental results of food dye and fluorescein solution (fluor) with DI-water, respectively. The measured average diffusivities were 6.62 × 10^{-10} m^2 s^{-1} and 5.17 × 10^{-10} m^2 s^{-1} (Fig. 2E), respectively. The corresponding standard deviations were 1.13 × 10^{-10} m^2 s^{-1} and 5.17 × 10^{-11} m^2 s^{-1}. Measured diffusivities were used for finite element analysis, and the mixing performance was studied under different flow rates and Reynolds numbers.

Data analysis

To quantify the mixing efficiency, ImageJ software was used to measure the intensity distribution of the mixed solution. The mixing efficiency was quantified by the mixing index (MI), and it was defined by the following equation:[27]

$$\mathrm{MI} = \frac{\sigma_{\mathrm{in}} - \sigma_{\mathrm{out}}}{\sigma_{\mathrm{in}}}, \quad (7)$$

where σ_{in} and σ_{out} represent the standard deviation of the concentration profile before and after the two solutions passed through the serpentine micromixer. For the colorimetric analysis of heavy metal ion detection, images of the mixed solution were converted into hue values to quantify the concentration level. Data analysis was conducted using Excel software, and student's t test was used for statistical analysis.

Fabrication of the SU-8 master

To create the master to mold the PDMS or the PP serpentine micromixer, a standard SU-8 master was fabricated. A 4″ silicon wafer was treated with piranha solution followed by a buffered-oxide etchant to remove the oxide surface layer. Then, a 50 μm or 60 μm thick SU-8 2050 (MicroChem) was spin-coated onto the wafer followed by a standard SU-8 photolithographic process. The exposure dosage was 230 mJ cm^{-2}, and this was higher than the recommended value of the vendor. Thus, the developed and hard baked SU-8 master had a

small draft angle for ease of demolding, particularly for removing plastic films.

Fabrication of the serpentine micromixer

Both PDMS and PP serpentine micromixers were fabricated. The fabrication process of the PDMS micromixer is briefly summarized in the following. First, a PDMS monomer and curing agent were mixed well in a 10-to-1 ratio followed by degassing in a vacuum chamber. Then, the PDMS micromolding process was conducted to form the serpentine microchannel from the SU-8 master. After baking in a 55 °C oven for four hours, the molded PDMS sheet was peeled off followed by O_2 plasma bonding to another PDMS sheet to seal the microchannel. The two inlets and one outlet were punched open with 21-gauge sharpened blunt needles to create through holes before the sealing step.

The VPM micromixer was made of a PP thin-film. We used a hot plate, air compressor and a vacuum pump to control the molding temperature and pressure. A pressure gauge and a thermocouple were used to monitor the molding process. The following is the developed hot embossing process. First, two 75 μm thick PP films and an SU-8 mold were placed in a molding chamber sealed with a 1 mm thick silicone rubber sheet. Then, the chamber was evacuated followed by increasing the chamber temperature to 165 °C. Once the temperature reached 140 °C, a positive pressure of 50 psi was applied to the thick rubber sheet to press the master into the softened PP film. The molding process was maintained at 50 psi and 165 °C for 20 minutes followed by cooling to 50 °C for demolding. The molded 150 μm thick PP film was sealed with a 100 μm thick PP sealing membrane for the PCR (Gunster Biotech Co., Ltd, Taiwan) to complete the thin-film micromixer. The sealing membrane was cut with a xerographic cutting machine (Graphtec, FC 4500-50) to make openings for fluid access before attaching to the hot embossed PP film.

Assembly of the VPM micromixer

Before sealing the thin-film micromixer inside the vacuum pouch, a 0.5 mm thick PDMS ring, a 0.5 mm thick PP ring or a 2 mm thick PMMA ring was attached around the exit of the micromixer to construct the storage reservoir using double-sided tape. Then, two ring-shaped pieces of double-sided tape with a 2 mm inner diameter ring were attached around the two entrances. This device was put inside a PP vacuum pouch and the evacuation process was initiated for 30 seconds. The opening of the vacuum pouch was sealed using an impulse sealer (Mercier Corporation, Me-200HI) to complete the assembly. Or, this device was put inside a Food Saver® vacuum seal bag and was pumped down to vacuum and sealed using a Food Saver machine (FM2000). The two ring-shaped pieces of tape at the two entrances attached to the inner surface of the vacuum pouch created a seal to separate the entrances from the evacuated cavity. Thus, once the vacuum pouch was pierced through the top of the entrances, reagents could be sucked into the micromixer and be mixed passively by the serpentine channel. The mixed solution flowed into the storage reservoir at the exit for observation, and it could be stored for post-processing.

Experimental setup

The operation procedure of the VPM micromixer was first to drop the food dye or the fluorescein solution on top of one of the entrances and to drop DI-water on top of the other entrance. Then, needles were used to make small holes in the vacuum pouch at the same time to initiate the mixing process. To make the two solutions flow into the two loading channels simultaneously, a 0.4 mm thick piece of stainless steel was machined using a laser cutting method to make two needles on one sheet. After the mixed solution was pumped into the reservoir, it could be stored for further examination or be analysed by the colorimetric method.

The volume flow rate and Reynolds number of the VPM micromixer in different driving modes and vacuum pouches were quantified by adding 4 μm red-fluorescent latex beads (FluoSpheres™) into DI-water. The velocity of these fluorescent beads was monitored in the straight microchannel near the exit of the micromixer. The travel distance within a fixed exposure time was measured to estimate the velocity and to calculate the volume flow rate and Reynolds number. Finally, the VPM micromixer was applied to perform mixing of potassium ferricyanide and ferrous ion solution. Three different levels of concentrations were mixed and quantified by the colorimetric method, including 10 ppm, 100 ppm and 1000 ppm. Mixing results were compared with the colorimetric data retrieved from loading premixed solutions into the VPM micromixer. Finally, the mixing process and colorimetric study were imaged using an inverted fluorescence microscope (Olympus, IX 71) and a fluorescence stereomicroscope (Zeiss, SteREO Discovery.V12).

3. Results

Pumping performance of the VPM system

Five different VPM micromixers were implemented for studying the performance of the VPM pumping system. Pumping methods in HP-, MP- and LP-modes were used for VPM micromixers sealed with the PP vacuum pouch, and they were labelled PP-HP, PP-MP and PP-LP, respectively. On the other hand, the HP-mode and MP-mode were developed for the VPM micromixer sealed in a Food Saver® vacuum seal bag. These were labelled FS-HP and FS-MP, respectively. The LP-mode conditions cannot be implemented due to the rib design of the vacuum seal bag. These ribs hindered the PDMS reservoir in forming conformal contact against the vacuum seal bag.

The pumping performance of the VPM mixers was quantified by tracing the volume flow rate (Q) over the mixing process. Fig. 3A summarizes the experimental results. It was found that the Re value of the VPM micromixers driven in the HP-mode was much larger than 10 for both PP and FS

vacuum pouches. This result suggests that the mixing mechanism for the HP-mode was dominated by chaotic advection. The mixing process could be completed within 3 seconds and within 7 seconds for PP-HP and FS-HP VPM micromixers, respectively. On the other hand, the major range of Re values for the MP-mode was between 1 and 10 except for the first 2 to 3 seconds. This suggests that the mixing performance for both PP-MP and FS-MP micromixers was in the most inefficient region of the serpentine micromixer, as verified by both finite element analysis (Fig. S1†) and experimental studies (Fig. S3†). The corresponding total time to complete the mixing process was 39 seconds and 1.7 minutes for PP-MP and FS-MP micromixers. Finally, the vacuum pressure of the PP-LP micromixer dropped rapidly during the initial 6 seconds and maintained a very low vacuum pressure for a long period of time. The total processing time could be longer than 10 minutes. The Re value was lower than 1 after 6 seconds, and the average Re value was 0.0064 with a standard deviation of 0.0095. This result suggests that the mixing mechanism was dominated by diffusion when driving the VPM micromixer in the LP-mode. Fig. 3B shows traced trajectories of fluorescent beads within a single exposure time, where the exposure time is labelled next to each condition. These results demonstrate that the back pressure can be adjusted to control the flow rate and Reynolds number using different designs of the reservoir at the exit.

Verification of long-term storage capability

To study the long-term storage capability, the flow rates of both PP and FS vacuum pouches were studied. It was found that the average flow rate of the VPM micromixer decreased to 22% in 24 hours when using the PP vacuum pouch (standard deviation was 10.5%). This could be due to the sealing quality of the impulse sealer not being ideal. In contrast, long-term storage was found to be feasible when using the commercial vacuum pouch sealing machine and vacuum seal bag (Food Saver®). Since the FS-HP VPM micromixer can provide a good mixing performance, the long-term storage study was conducted by using this device. Fig. 3C shows the experimental results. Re values for the first 10 seconds were quantified at different time points after sealing, including 10 minutes, 1 day, 7 days, 14 days, 21 days, and 28 days. Note that the number of quantified time points was lower for results from a shorter storage time. This was due to the vacuum pressure being larger and the overall processing time being faster. The experimental finding suggests that the vacuum pressure can be maintained up to 14 days with no significant difference. The Re value can be maintained well above 10 throughout the mixing process. After 21 days, the operating Re value started to display a significant difference with respect to the 10 minute data. The average Re values decreased to 60.5% and 53.5% for day-21 and day-28, respectively. The average Re values for the day 21 case were still higher than 10 for the first 10 seconds but were near 10 for the day-28 case. This experimental result suggests that using the commercial machine and vacuum seal bags, the VPM micromixer could be stored for 4 weeks to provide a sufficient flow rate for mixing applications.

Effect of viscosity of the fluid on the VPM system

To further study the performance of the VPM-based pumping system, different mixtures of DI-water and glycerol were used to change the fluid viscosity (η) from 1 cP (100% DI-water) to 60.1 cP (glycerol 80% v/v). Fig. 4 shows the set of experimental results to study the effect of the viscous fluid using the FS-HP VPM micromixer. Fig. 4A shows the measured volume flow rates (Q) in each condition. The average Q value was the highest with pure DI-water, and it decreased along with a higher percentage of glycerol. The reduction rate of the Q value over time was much slower for the highly viscous fluid. For the case of 80% glycerol (v/v), the vacuum pressure can last for more than 200 seconds to maintain the fluidic flow. The correlation between the average Q (black line) and viscosity η (grey line) is summarized in Fig. 4B. The reduction percentage of the average flow rate Q with respect to pure DI-water (1 cP) was 51.1%, 29.5%, 10.5% and 3.1% for 1.76 cP

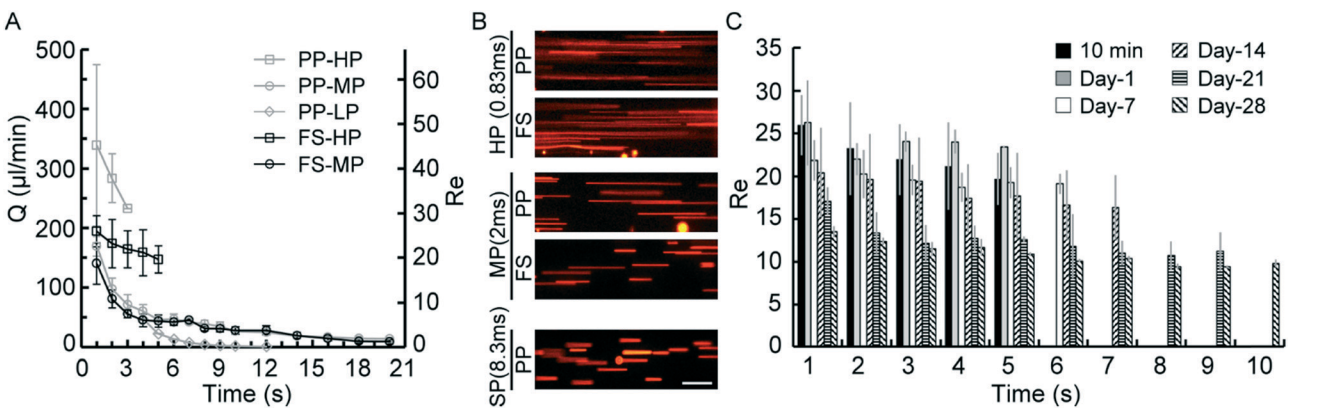

Fig. 3 (A) Measured volume flow rate Q and Reynolds number Re of 5 different types of VPM micromixers driven in three different modes. (B) Micrographs of red fluorescent beads flowed in each type of micromixer (scale bar = 100 μm). (C) Quantified Reynolds number of FS-HP micromixers operated at different time points during a 28 day storage period.

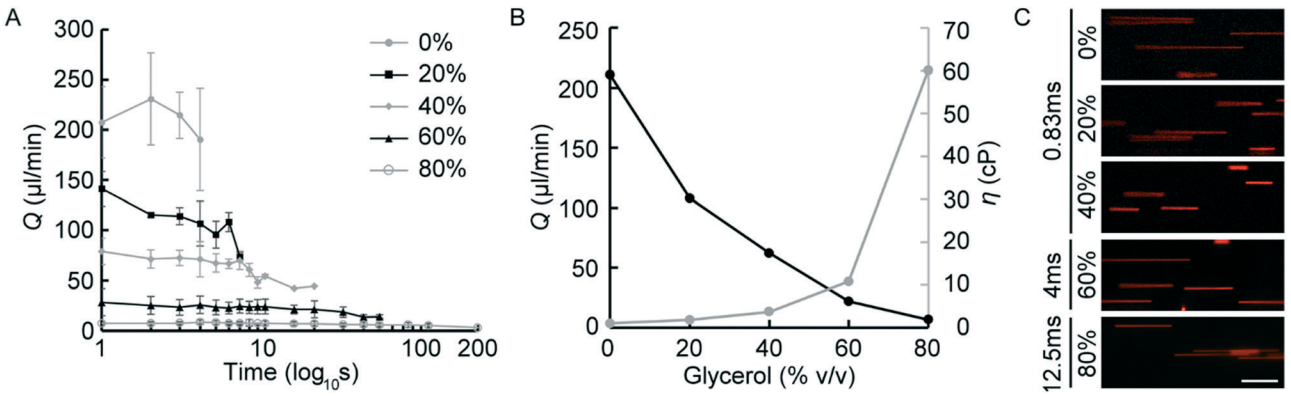

Fig. 4 (A) Traced volume flow rate Q of different DI-water and glycerol mixtures for studying the pumping performance of the VPM micromixer. FS-HP micromixer was used. (B) The correlation between the averaged Q value and viscosity η. (C) Micrographs of red fluorescent beads flowed in fluids with different glycerol percentages (scale bar = 100 μm).

(20% v/v), 3.72 cP (40% v/v), 10.8 cP (60% v/v) and 60.1 cP (80% v/v) viscous fluids, respectively. This effect can be observed from the trajectories of fluorescent beads within a single exposure time, as shown in Fig. 4C. Note that the exposure time was longer for the conditions with higher viscous fluids. These fluorescence images demonstrate that the traveling distance of fluorescent beads is reduced significantly for fluids with higher viscosity.

Mixing performance of the VPM micromixer

The mixing performance of the VPM micromixers in three different driving modes was investigated, and their mixing patterns were compared with the results retrieved from the PDMS micromixer. The serpentine channel with 20 obstacles was used in this study. Fig. 5A–F show the loading process of the MP-mode VPM micromixer. Since the two loading channels cannot be completely identical and the initiation of the piercing process cannot be perfectly synchronized, one of the solutions to be mixed was always sucked into the microchannel first and the other one caught up quickly. This step is shown in Fig. 5A–C (phase 1). Once both solutions had been sucked into the serpentine channel, the flow rate could be maintained within a small range and the mixing process was performed passively (phase 2). At the final stage (phase 3), the droplet size of the two solutions became very small so the surface tension could influence the pressure gradient between the two loading channels, and the flow pattern could become unstable and start to wiggle periodically, as shown in Fig. 5D and E. Finally, the mixing process was terminated once one of the solutions was depleted and air was sucked into the serpentine channel (Fig. 5F). The percentages of the processing time for these three phases were 3.9%, 68.6% and 27.5% for the MP-mode. The ratio of phase 2 for LP- and HP-modes can be higher since the LP-mode was operated at low pressure and the HP-mode was driven under a high flow rate.

To study the mixing mechanism of the VPM micromixers with two different vacuum pouches and three driving modes, the mixing pattern was investigated and compared with that of the PDMS micromixer. Fig. 5G shows the corresponding mixing patterns of the fluorescein solution mixed by PP-LP,

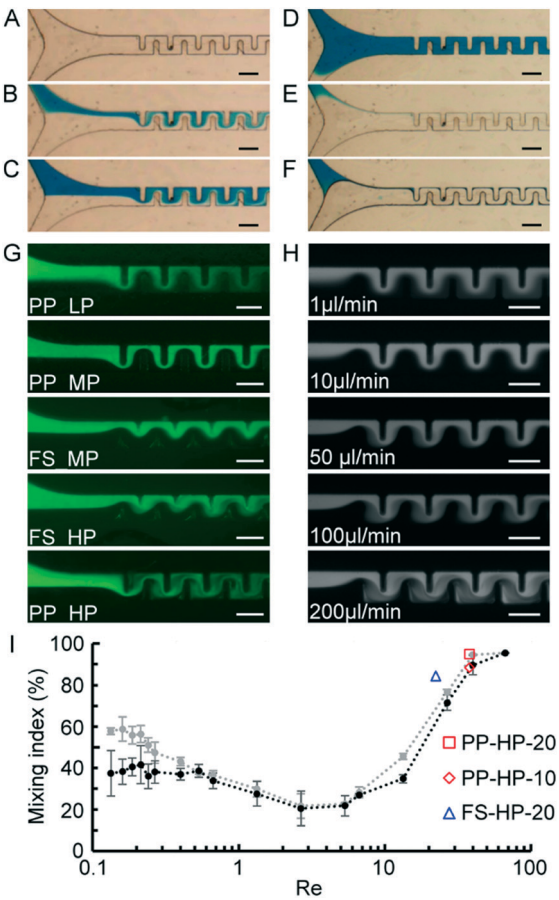

Fig. 5 (A–F) Sequential images of the loading process of the PP-MP VPM micromixer. (G and H) Fluorescence micrographs of mixing patterns of 5 different VPM micromixers (G) and mixing patterns of the PDMS micromixer driven by 5 levels of volume flow rates (H) (scale bar = 200 μm). (I) Measured mixing index (MI) for PDMS micromixers with 10 (black dotted line) and 20 (grey dotted line) obstacles. The red box, red diamond and blue triangle are the MI values of PP-HP-20, PP-HP-10 and FS-HP-20, respectively.

PP-MP, FS-MP, FS-HP and PP-HP VPM micromixers, and Fig. 5H shows the mixing patterns of the PDMS micromixer driven under 1 μl min^{-1}, 10 μl min^{-1}, 50 μl min^{-1}, 100 μl min^{-1} and 200 μl min^{-1}. The mixing pattern of the PP-LP micromixer demonstrated that the flow rate was slow and diffusion was the dominant mixing mechanism, verifying that it was driven in a low Re range. Its pattern was similar to that of the PDMS micromixer driven at 1 μl min^{-1}. In contrast, the flow rate of the two HP-mode VPM micromixers was much higher and reached a high Re value. Chaotic advection dominated the mixing mechanism, where folding and vortices were observed. The mixing patterns of FS-HP and PP-HP micromixers were close to the PDMS micromixer driven at 100 μl min^{-1} and 200 μl min^{-1} flow rates, respectively. The flow patterns of PP-MP and FS-MP micromixers were similar to those of the PDMS micromixer driven at 10 μl min^{-1} and 50 μl min^{-1}, respectively. They were in the region between Re equal to 1 and 10, where diffusive and chaotic mixing mechanisms were not strong enough to perform a complete mixing process.

Finally, since the HP-mode VPM micromixer had the most efficient mixing performance and the shortest processing time, the mixing indices for both PP-HP and FS-HP micromixers were investigated. It was found that the mixing index of the PP-HP micromixer with 10 obstacles was 88.3% with a standard deviation of 2.4%. The mixing performance was further improved using the VPM micromixer with 20 obstacles. The mixing index reached 94.9% with a standard deviation of 0.3%. The mixing index of the FS-HP micromixer with 20 obstacles was 84.4% with a standard deviation of 1.2%. The lower mixing performance of the FS-HP micromixer than that of the PP-HP one was due to the operating Reynolds number being about 63.1% lower. These results met the analysis of mixing indices for the PDMS micromixer, as shown in Fig. 5I. The black and grey dotted lines are quantified mixing indices of PDMS serpentine micromixers with 10 and 20 obstacles, respectively. The biphasic distribution is evident. The measured mixing indices of the PP-HP micromixer with 20 and 10 obstacles are labelled with a red box (PP-HP-20) and a red diamond (PP-HP-10), respectively. Their values match the result of the PDMS micromixer very well. The mixing index of the FS-HP micromixer is also labelled with a blue triangle (FS-HP-20). Its value is slightly higher than the result of the PDMS micromixer, but it has a similar trend on the dependency on the Reynolds number with respect to PP-HP.

Detection of ferrous ion concentration by the VPM micromixer

Fig. 6 shows the feasibility study of the VPM micromixer for heavy metal ion detection. A colorimetric assay was used to quantify the concentration of the ferrous ion solution. The integration of colorimetric detection was because the quantitative analysis can be conducted using a standard portable device equipped with a high resolution digital camera, such as a smartphone or a tablet computer. Fig. 6A shows an image of the PP-HP VPM micromixer used in this study, where 0.1 M potassium ferricyanide solution was used to react with a 1000 ppm ferrous ion solution made of $FeSO_4$. This shows that the mixed solution can be collected and imaged at the reservoir. Fig. 6B–D show the experimental results of using the VPM micromixer to detect 10 ppm, 100 ppm and 1000 ppm ferrous ion solutions. The two-order difference in the concentration can be observed from the reaction color. The concentration of the ferrous ion can be quantified by converting the color tone to hue values. Fig. 6E shows the result of the colorimetric analysis. White boxes denote the results of the VPM micromixer, and grey boxes denote the reference values by loading the premixed solution into the VPM micromixer. This result demonstrates that the VPM micromixer can be used to detect ferrous ion concentration in two orders of magnitude. Finally, to make the single-step loading process a user-friendly interface, a simple piercing apparatus was constructed by placing a dual-needle stainless steel plate in a stapler. This stapler can be used to pierce two loading channels at almost the same time to initiate the mixing process, as shown in Fig. 6F–H. Fig. 6I is an image of the dual-needle design installed in a stapler, and Fig. 6J shows an image of one of the two needles, where the needle length is 0.27 mm to prevent piercing through the bottom layer of the micromixer. A video (Video-S1†) is also provided.

4. Discussion

For the past two decades, a variety of lab-on-a-chip systems have been developed for point-of-care diagnostics,

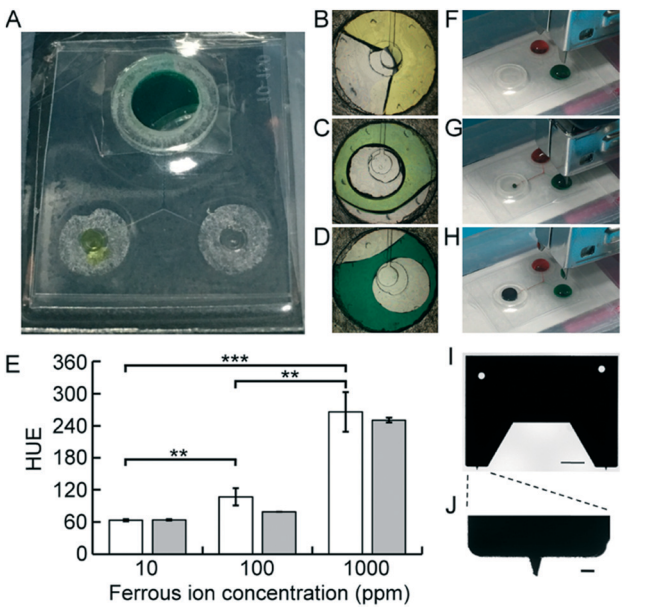

Fig. 6 (A–H) An image of the VPM micromixer for colorimetric detection of ferrous ion concentration (A), and images of potassium ferricyanide solution mixed with 10 ppm (B), 100 ppm (C) and 1000 ppm (D) ferrous ion solutions. (E) Colorimetric analysis of the mixed solution (white boxes), and the comparison with premixed solutions (grey boxes). (F–H) Sequential images of using a stapler to initiate the loading process. (I and J) An image of the dual-needle stainless steel sheet (I), and a zoom-in of one needle, where scale bars are 2 mm and 250 μm, respectively.

environmental analysis and food safety. Nevertheless, to transfer laboratory-made devices to commercial products for practical use is a big challenge and is a long path to success. Possible reasons can be summarized as follows: (1) complexity, as multiple active components are needed for operation; (2) external support, as an external system is required for operation and power; (3) fabrication, as the configuration of the microfluidic design cannot be reproduced easily by industrial processes; (4) cost, as the complexity of the design and the requirement of an external support can be limiting factors; (5) user experience, as the level of operation complexity and size/weight of the overall system can be a determining factor for acceptance and prevalence for end-users. Among these 5 reasons, the user experience is considered to be the most important factor since a user-friendly interface, lightweight and portability are the highest concerns.

In view of these considerations, the recent trend of portable lab-on-a-chip devices has moved to simple, rapid, lightweight and affordable systems, as seen in hand-powered self-contained microfluidic systems.[9–19] The general concerns of end users and laboratory-to-industry were also addressed by Whitesides[28] and many other papers.[29,30]

In order to shorten the path from laboratory to practical applications, we put together the considerations of the pumping method, microfluidic configurations, fabrication, user experience and cost to the design of the VPM system. It is summarized in the following.

First, the size and weight are decreased substantially when using a vacuum pouch and passive microfluidic design, which we demonstrated with a passive serpentine micromixer in this paper. Thus, an external support or an external fixture like a syringe, balloon or a pumping lid is not needed. It is lightweight since both the vacuum pouch and the microfluidic device are made of plastic thin films.

Second, to minimize the hurdles of transferring the microfluidic design to industrial fabrication methods, we chose the serpentine micromixer design that can be easily scaled up to metal masters for mass production. In addition, to enable roll-to-roll processing,[31] both the microfluidic device and the on-chip pump are made of plastic thin-films that can be mass produced by standard hot embossing and vacuum pouch sealing processes.

Third, the control of the flow rate is very straightforward, as we demonstrated with the micromixer. By changing the back pressure induced by the storage reservoir, we can generate flow rates of 4 orders of magnitude without the need to change the design of the on-chip pump and the microfluidic design. This is by far the largest range for on-chip pumps to the best of our knowledge.

Finally, but most importantly, a user-friendly interface is developed. The design to improve user experience includes: (1) the VPM device is a thin-film laminated plastic chip, which is lightweight and disposable. (2) The on-chip pump is already embedded, which is hassle-free for users since they do not need to figure out how to assemble it. (3) The operation only requires two simple steps, loading and piercing. The loading can be easily controlled by treating the surface of the vacuum pouch to have a hydrophilic surface only at entrance areas and use a standard pipette or a dropper with a controlled volume for loading. The initiation step can be simple, as we demonstrated. A small handheld apparatus like a stapler with a roll of needles like in Fig. 6I can be used to perform multiple tests, where the needle can be disposed of without touching it. Furthermore, the needles are very small (0.27 mm) and can minimize potential hazards. (4) The VPM system is robust. Since the microfluidic design is passive, the process can be done passively once it is activated.

In summary, the VPM system uses laminated plastic film to incorporate both microfluidic devices and a vacuum pump. It is a user-friendly device for on-site detection with the advantages of being standalone and portable, lightweight and flexible, disposable and low cost, with a long shelf-life.

Conclusions

In this paper, a new type of lab-on-a-chip system, called a vacuum pouch microfluidic (VPM) system, is presented. Its performance is demonstrated with a VPM micromixer. The overall system was constructed from a vacuum pouch and a thin-film micromixer that used a serpentine channel to perform passive mixing. Excluding the storage reservoir at the exit, the overall thickness of the VPM micromixer was 0.4 mm and the overall weight was 0.3 g. The operation procedure has only two steps: loading reagents and piercing the vacuum pouch to initiate the mixing process. To demonstrate that the level of stored negative pressure can be adjusted, three different reservoirs were designed to control the volume flow rate and the resultant Reynolds number. It was verified that the average velocity can be as low as 0.048 $\mu l\ min^{-1}$ and as high as 338.8 $\mu l\ min^{-1}$, resulting in a wide range of Re values from 0.0064 to 45.2. Thus, the range of Reynolds numbers can span 4 orders of magnitude when using the VPM system. The capabilities of performing long-term storage and handling highly viscous fluids were also verified when using a commercial machine and vacuum seal bags. The VPM micromixer can be stored for at least 4 weeks and can provide sufficient vacuum pressure for mixing applications. The performance of the VPM micromixer was also analysed and verified by finite element analysis and using a PDMS micromixer with an identical serpentine channel. It was found that the mixing mechanism was biphasic, where diffusion and chaotic advection contributed mainly for $Re < 1$ and $Re > 10$, respectively. Finally, the feasibility of applying this VPM micromixer for on-site detection of heavy metal ions was demonstrated, and concentrations of 10 ppm, 100 ppm and 1000 ppm can be detected and quantified by incorporating a colorimetric detection method. In summary, the present VPM system offers a new platform that has superior characteristics of flexibility, being lightweight, disposability and having low cost. Its fabrication process is compatible with industrial processes, and it can have a long shelf-life since its negative pressure can be sealed by the vacuum pouch. A simple apparatus like a

stapler is sufficient to initiate the process, and a portable device like a smartphone can be used to perform quantitative analysis.

Author contributions

Yu-Hsiang Hsu designed the research and experimental methods. Cheng-Je Lee designed and fabricated the VPM-micromixer, and he conducted the experiments, finite element analysis and data analysis. Both authors wrote the manuscript.

Conflicts of interest

There are no conflicts to declare.

Acknowledgements

This work was supported by the Ministry of Science and Technology, Taiwan (R.O.C) (MOST 106-2628-E-002-002-MY3).

References

1 C. D. Chin, V. Linder and S. K. Sia, *Lab Chip*, 2012, **112**(12), 2118–2134, DOI: 10.1039/C2LC21204H.
2 J. Wu, M. Dong, C. Rigatto, Y. Liu and F. Lin, *NPJ Digit. Med.*, 2018, **1**, 7, DOI: 10.1038/s41746-017-0014-0.
3 A. H. C. Ng and A. R. Wheeler, *Clin. Chem.*, 2015, **61**(10), 1233–1234, DOI: 10.1373/clinchem.2015.240226.
4 A. Jang, Z. Zou, K. K. Lee, C. H. Ahn and P. L. Bishop, *Meas. Sci. Technol.*, 2011, **22**, 032001, DOI: 10.1088/0957-0233/22/3/032001.
5 B. C. Dhar and N. Y. Lee, *BioChip J.*, 2018, **12**(3), 173–183, DOI: 10.1007/s13206-018-2301-5.
6 A. Jang, Z. Zou, K. K. Lee, C. H. Ahn and P. L. Bishop, *Meas. Sci. Technol.*, 2011, **22**, 032001, DOI: 10.1088/0957-0233/22/3/032001.
7 L. Guo, J. Feng, Z. Fang, J. Xu and X. Lu, *Trends Food Sci. Technol.*, 2015, **46**, 252e263, DOI: 10.1016/j.tifs.2015.09.005.
8 M. Boyd-Moss, S. Baratchi, M. Di Venerec and K. Khoshmanesh, *Lab Chip*, 2016, **16**, 3177–3192, DOI: 10.1039/c6lc00712k.
9 K. Iwai, K. C. Shih, X. Lin, T. A. Brubaker, R. D. Sochol and L. Lin, *Lab Chip*, 2014, **14**, 3790–3799, DOI: 10.1039/c4lc00500g.
10 A. Chen and T. Pan, *Lab Chip*, 2014, **14**, 3401–3408, DOI: 10.1039/c4lc00540f.
11 K. Han, Y. –J. Yoon, Y. Shin and M. K. Park, *Lab Chip*, 2014, **16**, 132–141, DOI: 10.1039/c5lc00891c.
12 P. Thurgood, J. Y. Zhu, N. Nguyen, S. Nahavandi, A. R. Jex, E. Pirogova, S. Baratchie and K. Khoshmanesh, *Lab Chip*, 2018, **18**, 2730–2740, DOI: 10.1039/c8lc00471d.
13 S. Begolo, D. V. Zhukov, D. A. Selck, L. Li and R. F. Ismagilov, *Lab Chip*, 2014, **14**, 4616–4628, DOI: 10.1039/c4lc00910j.
14 I. K. Dimov, L. Basabe-Desmonts, J. L. Garcia-Cordero, B. M. Ross, A. J. Ricco and L. P. Lee, *Lab Chip*, 2011, **11**, 845–850, DOI: 10.1039/c0lc00403k.
15 A. W. Martinez, S. T. Phillips and G. M. Whitesides, *Anal. Chem.*, 2010, **82**, 3–10, DOI: 10.1021/ac9013989.
16 Y. Yang, E. Noviana, M. P. Nguyen, B. J. Geiss, D. S. Dandy and C. S. Henry, *Anal. Chem.*, 2017, **89**, 71–91, DOI: 10.1021/acs.analchem.6b04581.
17 N. M. Rodriguez, W. S. Wong, L. Liu, R. Dewar and C. M. Klapperich, *Lab Chip*, 2016, **16**, 753–763, DOI: 10.1039/c5lc01392e.
18 T. Kokalj, Y. Park, M. Vencelj, M. Jenko and L. P. Lee, *Lab Chip*, 2014, **14**, 4329–4333, DOI: 10.1039/c4lc00920g.
19 J. Hu, S. Wang, L. F. Wang, B. Pingguan-Murphy, T. J. Lu and F. Xu, *Biosens. Bioelectron.*, 2014, **54**, 585–597, DOI: 10.1016/j.bios.2013.10.075.
20 K. –W. Lin and J.-T. Yang, *Int. J. Heat Mass Transfer*, 2007, **50**, 1269–1277, DOI: 10.1016/j.ijheatmasstransfer.2006.09.016.
21 N. –T. Nguyen and Z. Wu, *J. Micromech. Microeng.*, 2005, **15**, R1–R16, DOI: 10.1088/0960-1317/15/2/R01.
22 S. Hossain and K.-Y. Kim, *Micromachines*, 2015, **6**, 842–854, DOI: 10.3390/mi6070842.
23 K. W. Oh, K. Lee, B. Ahn and E. P. Furlani, *Lab Chip*, 2012, **12**, 515, DOI: 10.1039/c2lc20799k.
24 C. J. Lee and Y. H. Hsu, *Int. conf. Smart Sensor* 2018, C1-00-0028.
25 C. J. Lee and Y. H. Hsu, *MicroTAS*, 2018, p. 3568.
26 H. Bruus, *Theoretical Microfluidics*, Oxford University press Inc., New York, New York, USA, 2008.
27 M. A. Ansari and K. Y. Kim, *Proc. 5th ICNMM*, 2007, p. 30054, DOI: 10.1115/ICNMM2007-30054.
28 G. M. Whitesides, *Lab Chip*, 2013, **13**, 11, DOI: 10.1039/c2lc90109a.
29 M. M. Gong, B. D. MacDonald, T. V. Nguyen, K. V. Nguyen and D. Sinton, *Lab Chip*, 2014, **14**, 957, DOI: 10.1039/c3lc51185e.
30 A. K. Yetisen, M. S. Akram and C. R. Lowe, *Lab Chip*, 2013, **13**, 2210, DOI: 10.1039/c3lc50169h.
31 M. Focke, D. Kosse, C. Muller, H. Reinecke, R. Zengerle and F. von Stetten, *Lab Chip*, 2010, **10**, 1365–1386, DOI: 10.1039/c001195a.